APPLICATIONS OF THE PERFECTLY MATCHED LAYER (PML) ABSORBERS

Y. Botros
J. Volakis

3rd Quarterly Report

Compact Software, Inc.
201 McLean Boulevard
Paterson, N.J. 07504

May 1997

PROJECT INFORMATION

PROJECT TITLE:	Accelerated 3D Arbitrary EM Simulation Methods
REPORT TITLE:	Applications of the Perfectly Matched Layer (PML) Absorbers
U-M REPORT No.:	034702-3-T
CONTRACT START DATE:	1 August 1996
END DATE:	31 July 1997
DATE:	May 1997 (3rd Quarterly Report)
SPONSOR:	Jason Gerber Compact Software, Inc. 201 McLean Avenue Paterson, N.J. 07504
SPONSOR CONTRACT No.:	96-0502
U-M PRINCIPAL INVESTIGATOR:	John L. Volakis EECS Department University of Michigan 1301 Beal Avenue Ann Arbor, MI 48109-2122 Phone: (313) 764-0500 Fax: (313) 647-2106 volakis@umich.edu http://www-personal.engin.umich.edu/~volakis/
CONTRIBUTORS TO THIS REPORT:	Y. Botros, J. Volakis

Applications of the Perfectly Matched Layers (PML) Absorbers

Youssry Y. Botros and John L. Volakis

Radiation Laboratory

Department of Electrical Engineering

and Computer Science,

The University of Michigan

Ann Arbor, MI 48109-2212

Abstract

The recently introduced perfectly matched uniaxial absorber layer (PML) for finite element meshes truncation has several advantages. Among them, its superior performance over the other truncation schemes such as the Absorbing Boundary Conditions (ABCs) and the isotropic material absorber scheme. Also, it offers ease of implementation since it can be included and implemented as part of the main mesh. It allows for code parallelization and it can be terminated conformally to the structure. In the first report, we discussed the theory of implementation for this absorber as well as its design characteristics. In the second one, we closely focused on the PML performance and optimization. We optimize the PML parameters in a way that achieves both faster convergence and higher absorption. Also, we performed a brief study on the different

solvers and preconditioning schemes. Based on these parametric studies, we now proceed by applying the optimized PML to several microwave examples representing actual and practical examples. These examples include a feed study for the microstrip lines, a coupling study for two parallel transmission lines on a substrate and a spiral inductor with an air bridge.

Contents

1 Introduction **3**

2 Numerical Deembedding **4**

3 Examples **6**

3.1 Feeding Study 6

3.2 Coupling study 7

3.3 Spiral with an air bridge 8

4 Conclusion **8**

1 Introduction

The need for an efficient way to truncate the computational domain for finite element method (FEM) applications led to the investigation of new anisotropic absorbers with reflectionless surfaces. These fictitious layers with uniaxial permittivity and permeability tensors offer several advantages. Among them, the avoid using the differential operators at the truncation boundaries, implementation ease and the promising conformal capabilities. Also, with these Perfectly Matched Layers (PMLs), there is no need for *a priori* knowledge of the propagation constants in the structure which may be difficult to obtain especially for complicated microwave circuits. The accuracy of this scheme is dependent on the optimal choice of the absorber layer parameters. In the first report [1] we introduced a brief introduction to the PML based on the theory developed in [17]. Also, we demonstrated different applications including radiation and scattering to demonstrate the PML superior performance over other truncation schemes. In the second report [2], we started to look at the optimization of the whole FEM system when the PML is used as a mesh truncation scheme. We tested several FEM simulators with several meshing and termination schemes and we noticed that most of the CPU time (90 % or more) is consumed in the solver (usually the iterative solver). Therefore, we addressed approaches for improving the solver performance. Specifically, the PML absorber parameters (attenuation and phase shift) are optimally selected to improve the convergence and hence reduce the number of iterations and CPU time. Using the optimal values, the PML is designed and implemented in the whole FEM mesh. Then, the FEM matrix is preconditioned using the simple diagonal preconditioner. Regarding solvers, we examined the performance of three different iterative solvers in terms of their implementation and convergence characteristics. In all cases, three dimensional simple examples were utilized to validate our

conclusions.

In this report, we present further studies for more complicated problems and structures. We performed a parametric study [1] and a PML optimization [2] to design and implement this termination scheme. Specifically, we considered three types of examples. The first is a feed study about the minimum number of probes required for achieve an accurate estimate of the input impedence after solving the FEM system of equations. Then, we discussed a simple coupling scheme between two microstrip lines printed on a dielectric substrate. Finally, we will presented our results for a spiral inductor geometry with an air bridge. To extract the various parameters from the FEM solution, we need a good and robust deembedding scheme. A brief mathematical summary about this technique is presented based on the transmission line analogy to circuits.

2 Numerical Deembedding

We are interested in the scattering parameters (S-parameters) for a uniform transmission line terminated by some load. For a shielded transmission line with a propagating wave in the y-direction (for example), the electric field vector along the line can be expressed as

$$E = E_i e^{-\gamma y} + E_r e^{\gamma y} \tag{1}$$

where E_i and E_r are proportional to the incident (incoming) and reflected (outgoing) waves and γ is the complex propagation factor. If we choose a reference plane at a certain distance (say y_o), the field at the a distances $+d$ and $-d$ from this reference plane are

$$E(d) = E_i e^{-\gamma d} + E_r e^{\gamma d} \tag{2}$$

$$E(0) = E_i + E_r \tag{3}$$

and

$$E(-d) = E_i e^{\gamma d} + E_r e^{-\gamma d} \tag{4}$$

Solving these three equations simultaneously, we obtain

$$cosh(\gamma\, d) = \frac{E(d) + E(-d)}{2E(0)} \tag{5}$$

from which we can determine quantities

$$\gamma = \alpha + j\,\beta \tag{6}$$

As usual α and β are the attenuation and phase shift coefficients in the pertinent section of the transmission line. We can also obtain the guided wave length and the effective dielectric constant from the following equations

$$\lambda_g = \frac{2\,\pi}{\beta} \tag{7}$$

$$\epsilon_{eff} = \sqrt{\frac{\lambda_o}{\lambda_g}} \tag{8}$$

with λ_o being the free space wavelength. The incident and reflected waves E_i and E_r are given by

$$E_i = \frac{E(0)\, e^{\gamma d} - E(d)}{2\, sinh(\gamma d)} \tag{9}$$

and

$$E_r = E(0) - E_i \tag{10}$$

Therefore, the reflection coefficient becomes

$$S_{11} = \frac{E_r}{E_i} \tag{11}$$

Although this deembedding process is suited for one port network analysis, the technique may be readily extended to two port and multiport networks. From the previous analysis and formulation, the S-parameters calculations is related directly to the termination scheme. Therefore, it is necessary and essential to have a good and accurate termination scheme such as the PML in order to extract the scattering parameters for different structures in an accurate and efficient way.

3 Examples

In this section, we present three different kinds of examples representing three different microwave structures. The first deals with the feeding of microwave circuits and filters. It examines the minimum number of feeding (current) probes required to maintain stable FEM calculations. The second example demonstrates the coupling between two parallel lines printed on dielectric substrate. One of these lines is directly fed and the amount of coupling to the other is calculated. Finally, a spiral inductor with an air bridge is considered as an application for the PML absorber. As shown in the previous report, the PML will be implemented with the optimal values of the parameters. A diagonal preconditioner used in the BiConjugate Gradient (BCG) solver to solve the linear system. It should be noted that the optimal value of the phase shift factor α for the absorber was near unity and the attenuation factor β was also almost unity.

3.1 Feeding Study

After studying the effects of the absorber parameters in the second report, we proceed to the input port where we model the feeding probes. We seek the minimum number of probes required to achieve a stable input impedence. To do this, we fix all parameters

of the circuit as well as the absorber and we change the number of feeding probes only. We change them from one to four and each time and examine the field value across each probe to calculate the input impedence. In our simulation, we discussed the effect of varying the number of probes on the input impedence. Figure 2 shows the input impedence calculation (real and imaginary) as a function of the number of probes. We notice the following:

1- The value of the real part of the input impedence is fairly constant and does not change much with the change in the probes number.

2- The imaginary part of the impedence depends strongly on the number of probes and decreases as the number of probes increases.

3- When the number of probes equals four, the imaginary part converges and therefore, we can deduce that four probes are enough or sufficient to extract an accurate input impedence from the finite element solution.

3.2 Coupling study

A preliminary study about coupling between two transmission lines in conjunction with the FEM method is presented in this section. As shown in figure 3, two transmission lines printed on a dielectric substrate represents our test case. The left transmission line is excited with all the rear end ports matched. The field under the second (right) transmission line is then obtained using the FEM model with optimized PML termination scheme. Figures 4- 6 show the coupling study when the left microstrip line is excited and the right one is kept parasitic. These figures display the variation of the real, imaginary and magnitude of the fields under both the active and parasitic lines. As displayed in the figures, the amount of coupling is increasing as we go deeper through the line. This is really expected because of the distributed capacitance between the two parallel conductors. The amount is a function of the

frequency, conductors separation and widths. For both excitation, we expect similar fields variation under the strip lines due to the symmetry in the problem. This is indicated in figure 7. Using the deembedding scheme discussed previously, we evaluated the scattering parameter S_{13} which represents the coupling of port #3 port #1 which has the feed probes. The magnitude of this factor is given in figure 10.

3.3 Spiral with an air bridge

We modeled the geometry shown in figure 9 using our FEM simulator with the PML termination. Our goal is to validate our code with the measured data for this geometry. As we observe in figure, this spiral has fine details to be considered. The results of the scattering parameter S_{11} are shown in figure 10 where there is a good agreement between the measured and calculated data. In the numerical simulation, to reduce the FEM size, we assumed that the width of the air bridge is equals that of the microstrip line.

4 Conclusion

In this report, we used development from the first and second reports to model actual circuits representing different problems and cases. We modeled the feed for microwave circuits and obtained the condition for reliable and accurate calculations. Also, we performed a preliminary study about the coupling between two transmission lines. In all of these studies, we used the optimized PML that was suggested in our second report. In the next quarter, we will examine spiral inductor antenna and we will consider more complicated examples representing circuits and filters. In the process, we will consider particularly the GMRES and CVSS solvers.

List of Figures

1 Microstrip Line 10

2 Input Impedence variation with the number of probes 11

3 Geometry of the Circuit for Coupling Studies 12

4 Real Parts of the Fields under the microstrip line for the active and parasitic lines 13

5 Imaginary Parts of the Fields under the microstrip line for the active and parasitic lines 14

6 Magnitude of the Fields under the microstrip line for the active and parasitic lines 15

7 Magnitude of the Fields under the microstrip line for the active and parasitic lines with both port excitation 16

8 Coupling Magnitude Between the two Lines as a Function of the excitation Frequency 17

9 Geometry of the spiral inductor with an air bridge 18

10 Magnitude of the scattering parameter S_{11} of the spiral antenna with an air bridge 19

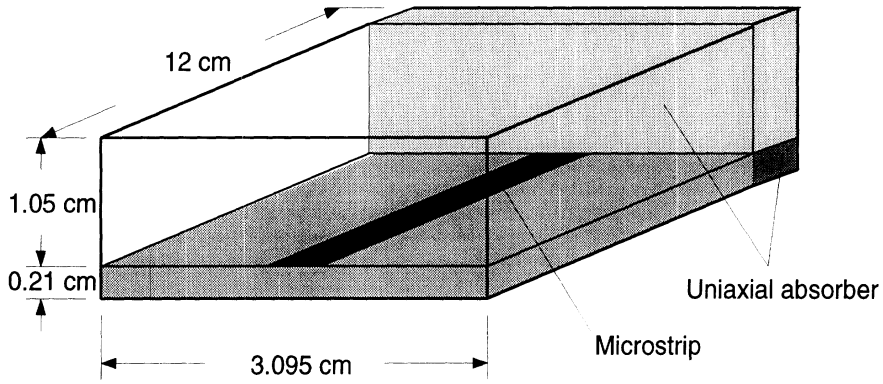

Figure 1: Microstrip Line

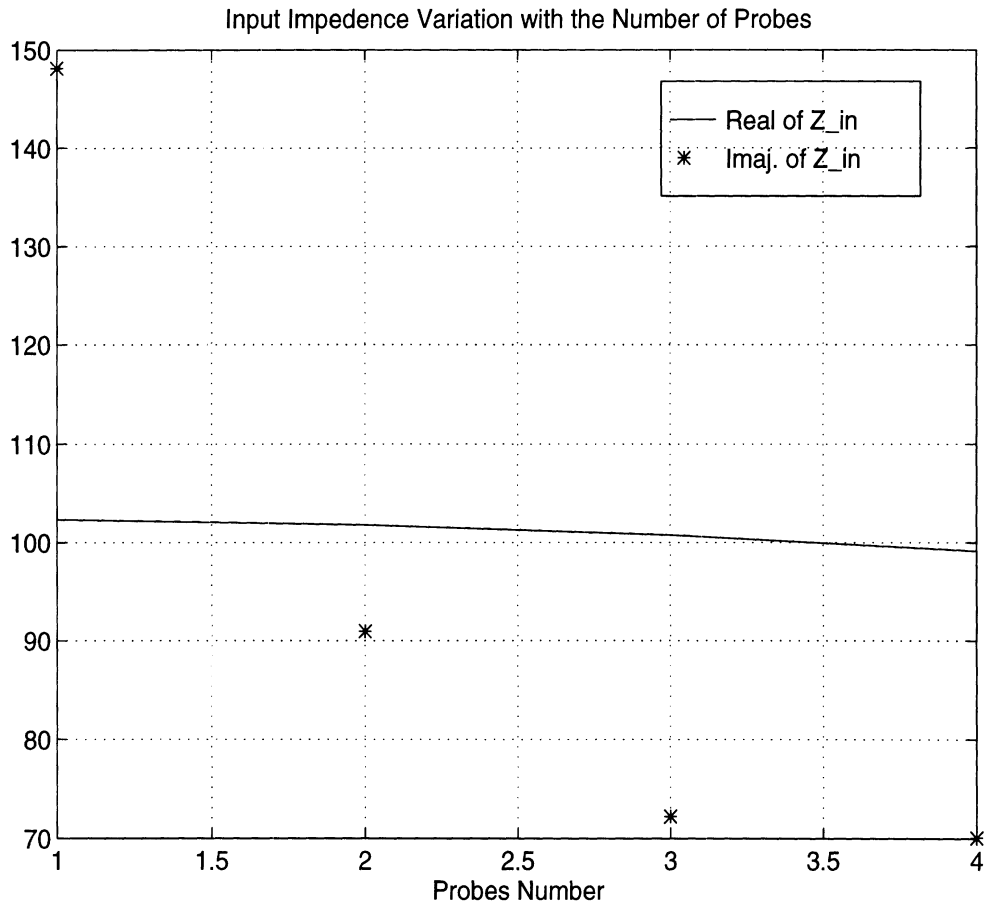

Figure 2: Input Impedence variation with the number of probes

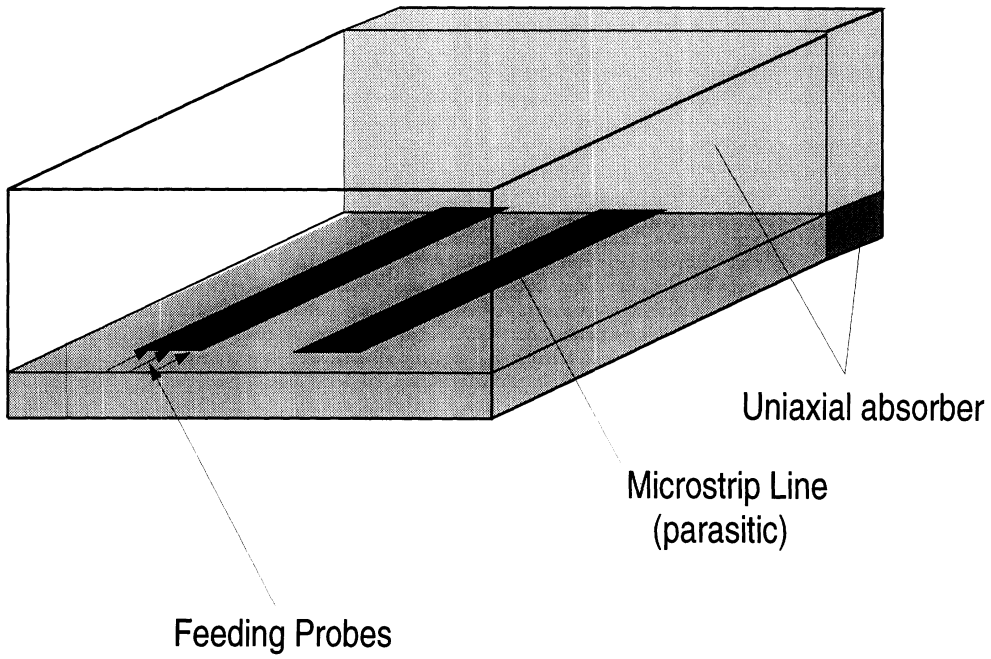

Figure 3: Geometry of the Circuit for Coupling Studies

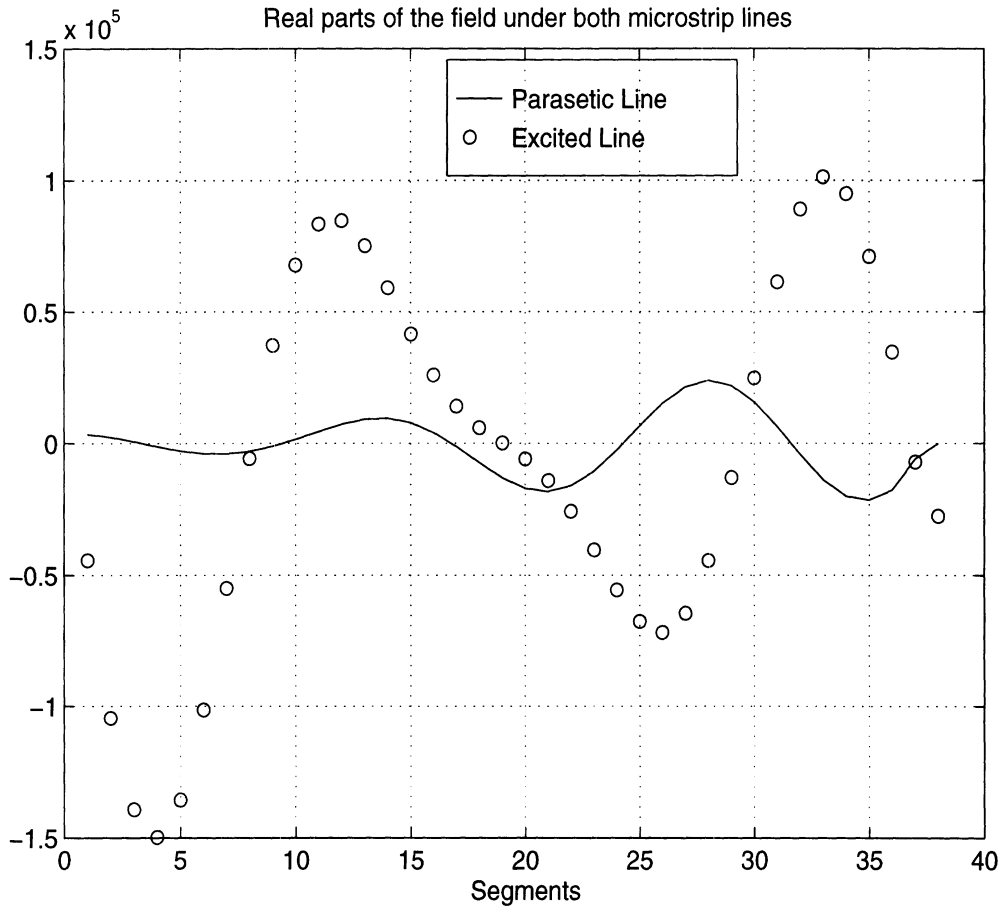

Figure 4: Real Parts of the Fields under the microstrip line for the active and parasitic lines

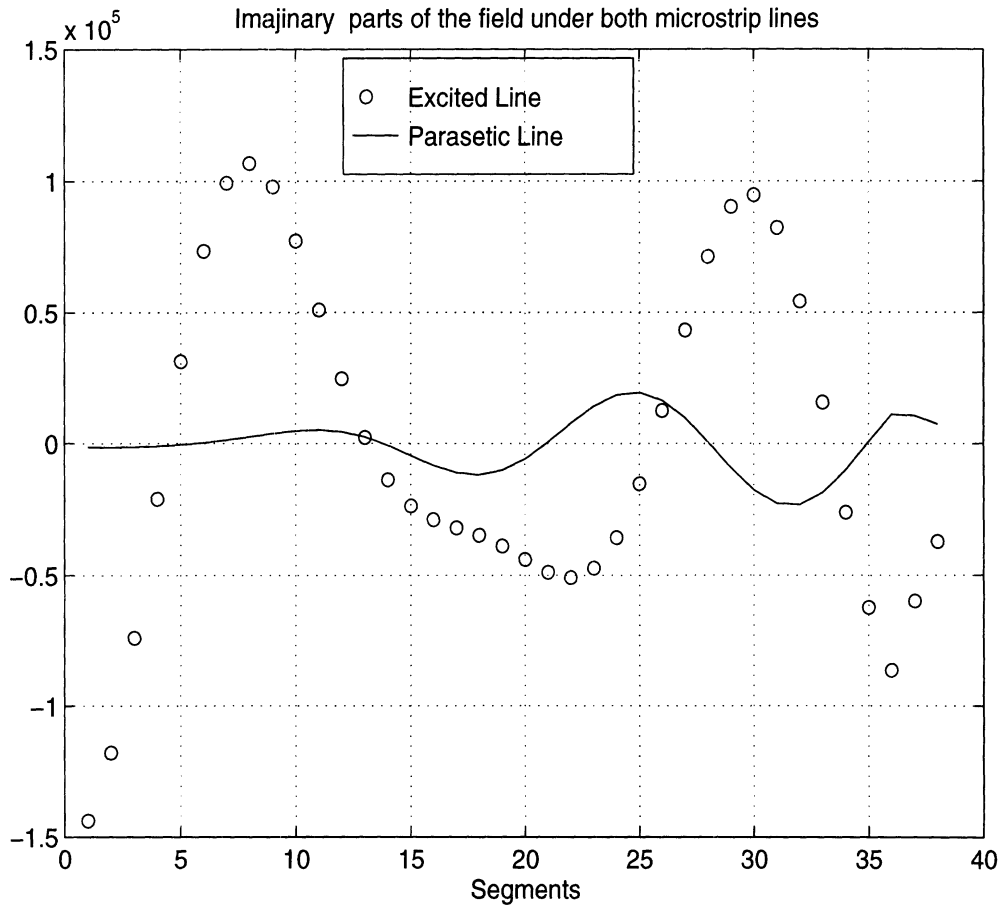

Figure 5: Imaginary Parts of the Fields under the microstrip line for the active and parasitic lines

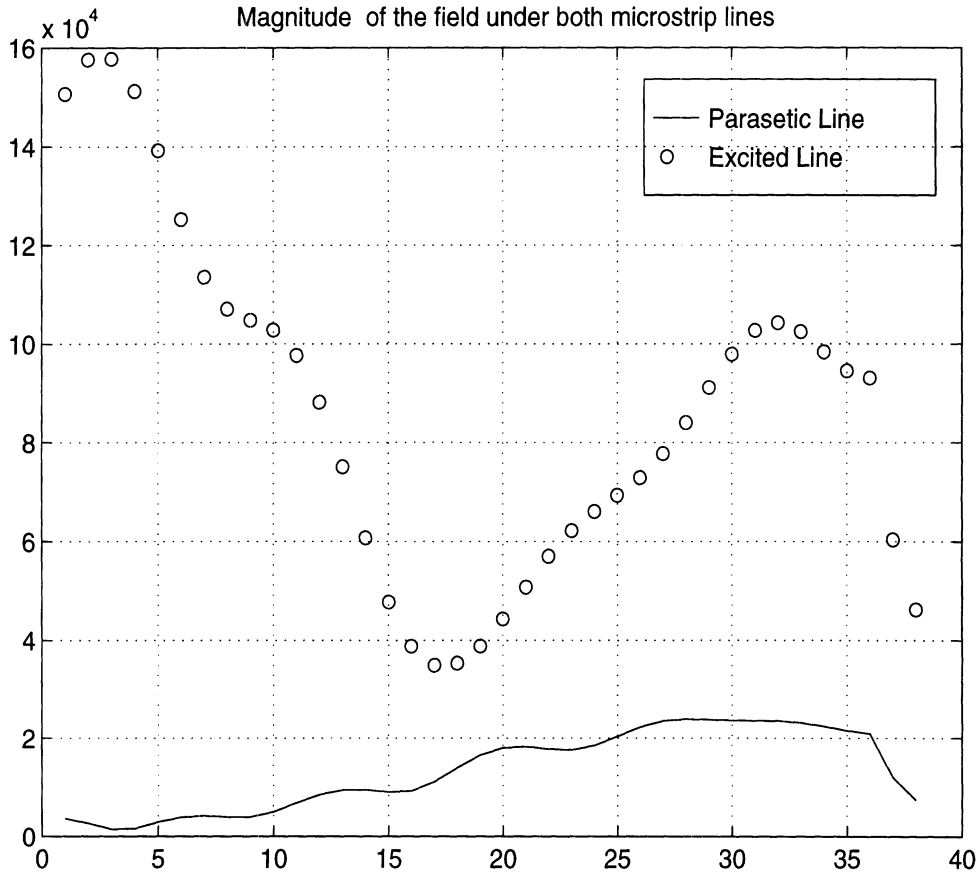

Figure 6: Magnitude of the Fields under the microstrip line for the active and parasitic lines

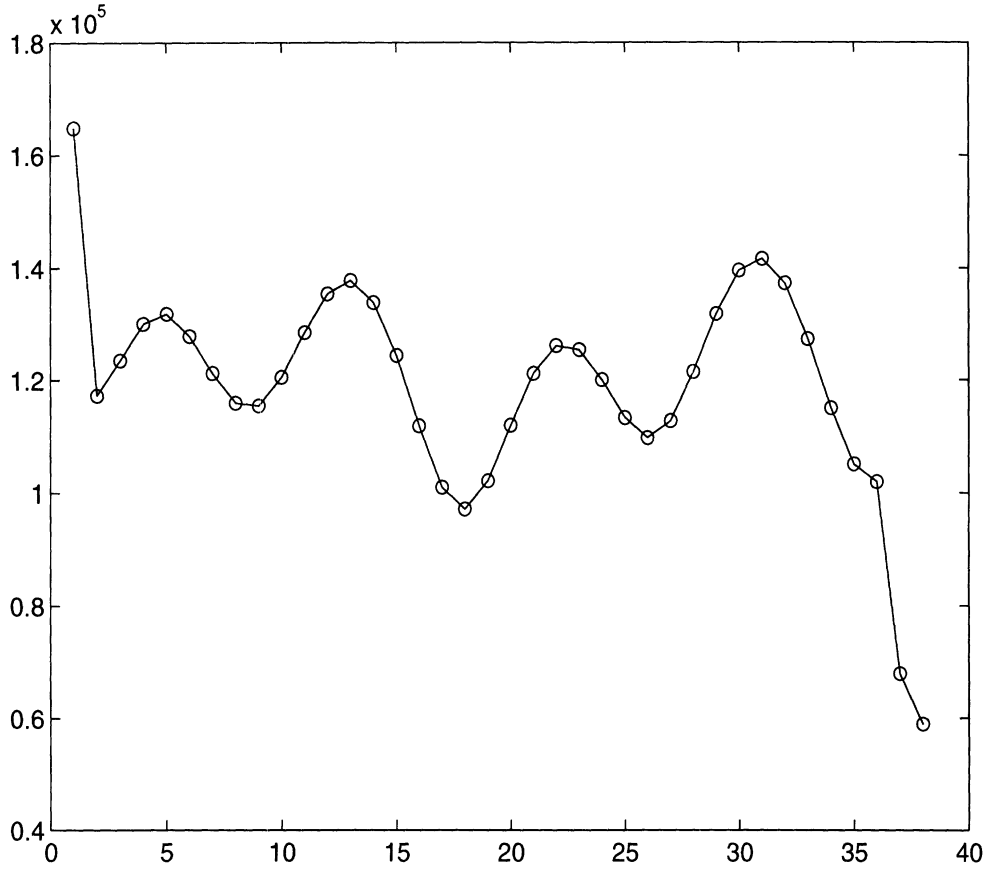

Figure 7: Magnitude of the Fields under the microstrip line for the active and parasitic lines with both port excitation

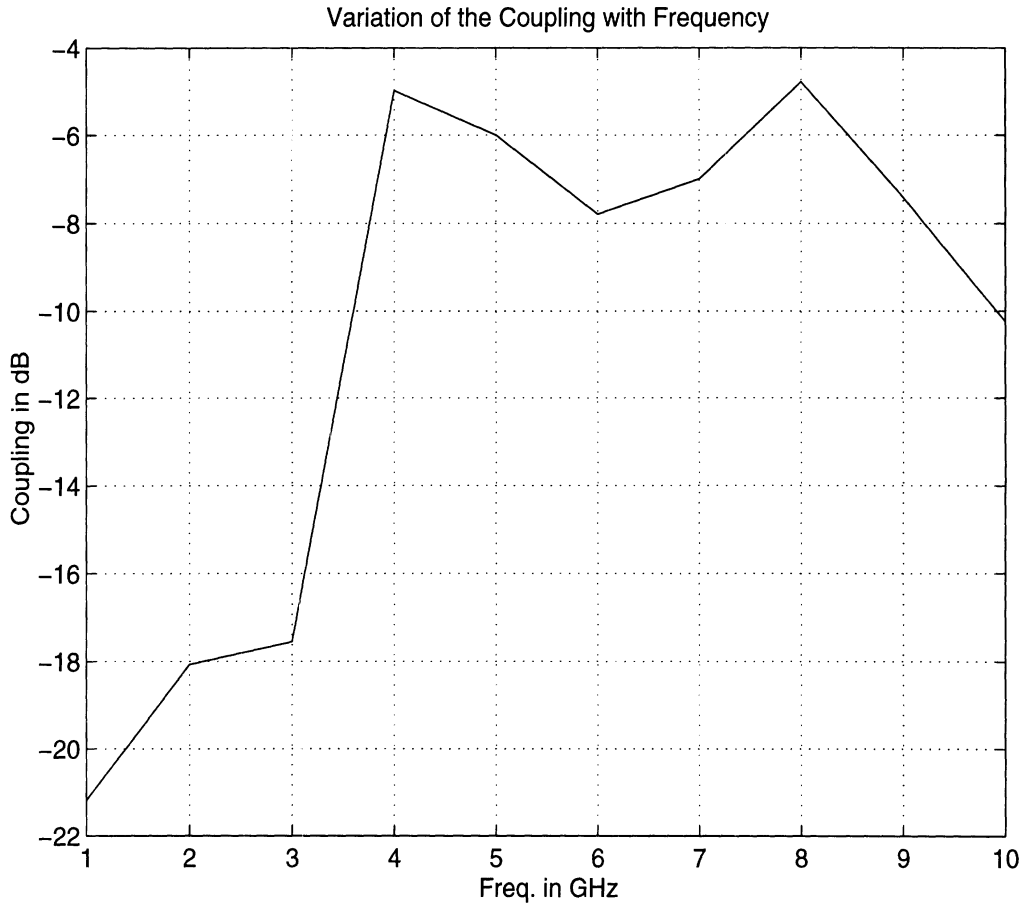

Figure 8: Coupling Magnitude Between the two Lines as a Function of the excitation Frequency

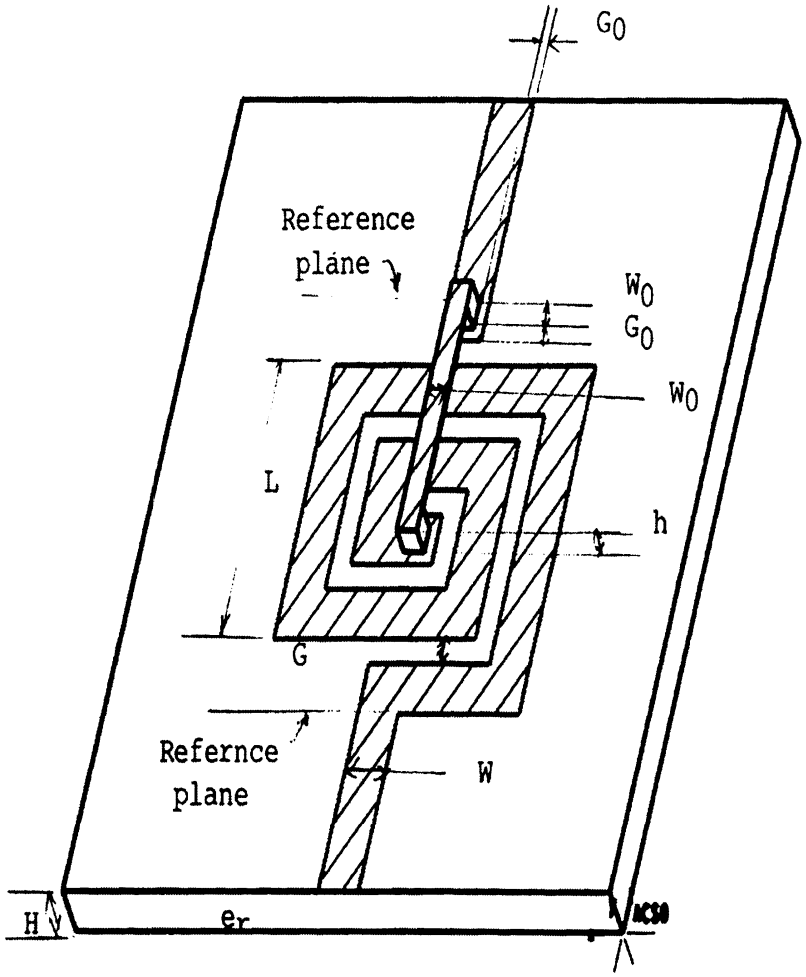

DIMENSION:

L = 3.4375 mm
G0 = 0.15625 mm
W_0 = 0.3125 mm
W = 0.625 mm
G = 0.3125 mm
H = 0.635 mm
h = 0.3125 mm
e_r = 9.8

Figure 9: Geometry of the spiral inductor with an air bridge

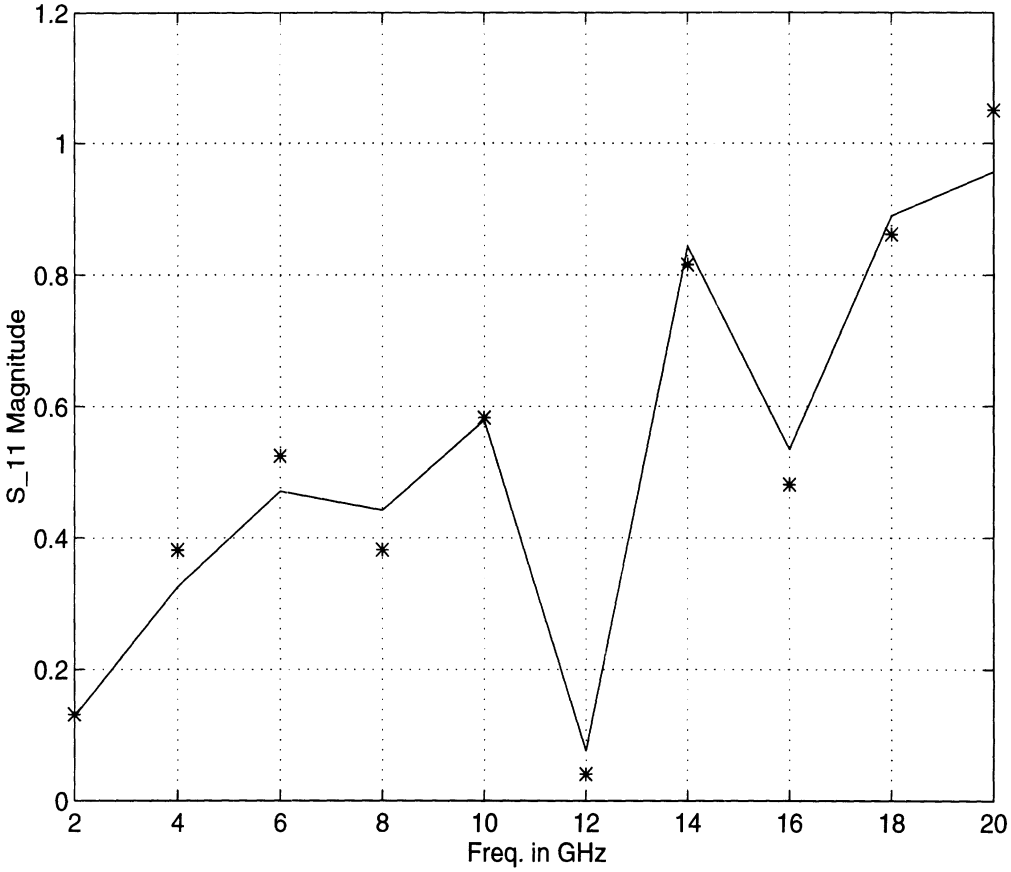

Figure 10: Magnitude of the scattering parameter S_{11} of the spiral antenna with an air bridge

References

[1] Y.Y. Botros, S.R. Legault, J. Gong, J.L. Volakis and T.B.A. Senior, "Perfectly Matched Absorbers (PML):Theory, Analysis and Implementation Radiation Laboratory Report (No. 034702-1), The university of Michigan, Ann Arbor, October 1996.

[2] Y.Y. Botros and J.L. Volakis "Convergence Study on FEM Systems with PML IMplementation" Radiation Laboratory Report (No. 034702-2), The University of Michigan, Ann Arbor, March 1997.

[3] B. Engquist and A. Majda, "Absorbing boundary conditions for the numerical simulation of waves," *Math. Comput.* Vol. 31, pp. 629–651, 1977

[4] L.Halpern and L.N. Trefethen, "Wide–angle one-way wave equations," *J. Acoust. Soc. Amer.* Vol. 84, pp. 1397–1404, 1988

[5] W. Sun and C.A. Balanis, "Vecter one–way wave absorbing boundary conditions for FEM applications," *IEEE Trans. Antennas Propagat.* Vol. AP–42, pp. 872–878, 1994

[6] Webb and Kanellopoulos, " Absorbing boundary conditions for the finite element solution of the vector wave equation," *Microwave Opt. Tech. Lett.* Vol. 2, pp. 370–372, 1989

[7] A. Chatterjee and J.L.Volakis, "Conformal absorbing boundary conditions for the vector wave equation," *Microwave Opt. Tech. Lett.* Vol. 6, pp. 886–889,1993

[8] R.L. Higdon, "Absorbing boundary conditions for acoustic and elastic waves in stratified media," *J. Comp. Phys.* Vol. 101, pp. 386–418, 1992

[9] Z.P. Liao H.L. Wong, B.P. Yang and Y.F. Yuan, "A transmitting boundary for transient wave analysis," *Sicentia Sinica* Vol. 28, pp. 1063–1076, 1984

[10] M. Moghaddam and W.C. Chew, "Stabilizing Liao's absorbing boundary conditions using single–precision arithmetic," it IEEE AP-S Int. Symp., London, Canada, pp. 430–433, 1991

[11] J.Fang, "ABCs applied to model wave propagation in Microwave integrated–circuits," *IEEE Trans. MTT*, Vol. 42, No. 8, pp. 1506–1513, Aug. 1994

[12] R. Luebbers and C. Penney, "Scattering from apertures in infinite ground planes using FDTD," *IEEE Trans. Antennas Propagat.* Vol. 42, pp. 731–735, May 1994

[13] B. Stupfel and R. Mittra, "Efficiency of numerical absorbing boundary conditions for finite element applications," *URSI Radio Science Meeting*, pp. 165, 1994

[14] K.K. Mei, R. Pous, Z. Chen, Y.W. Liu and M.D. Prouty, " Measured equation of Invariance: A new concept in field computations," *IEEE Trans. Antennas Propagat.* Vol. 42, pp. 320–328, March 1994

[15] T. Özdemir and J.L.Volakis, "A comparative study of an absorbing boundary condition and an artificial absorber for truncating finite element meshes," *Radio Science* Vol. 29, No. 5, pp. 1255–1263, Sept. 1994

[16] J.-S. Wang and R. Mittra, "Finite element analysis of MMIC structures and electronic packages using absorbing boundary conditions," *IEEE Trans. Microwave Theory and Techn.*, Vol. 42, pp. 441-449, March 1994.

[17] Z.S. Sacks, D.M. Kingsland, R. Lee and J.F. Lee, "A perfectly matched anisotropic absorber for use as an absorbing boundary condition," *IEEE Trans. Antennas and Propagation*, December 1994.

[18] Berenger, J.P. "A Perfectly Matched Layer for the Absorption of Electromagnetic Waves," *J. Comp. Physics*, 114 : 185-200, 1994.

[19] Chew, W.C. and Weedon, W.H. "A 3-D Perfectly Matched Medium from Modified Maxwell's Equations with Stretched Coordinates," *Microwave and Optical Technology Letters*, p.599-604. September, 1994.

[20] Katz, D.S, Thiele, E.T., and Taflove, A. "Validation and Extension to Three Dimensions of the Berenger PML Absorbing Boundary Condition for FD-TD Meshes," *IEEE Microwave and Guided Wave Letters*, August, 1994, p.268-270.

[21] C. Rappaport and L. Bahrmasel, "An absorbing boundary condition based on anechoic absorber for EM scattering computation," *J. Electromagn. Waves Appl.*, Vol. 6, No. 12, pp. 1621-1634, Dec. 1992.

[22] R. R. Bonetti and P. Tissi, "Analysis of Planar Disk Networks", IEEE MTT-26, July 1978, pp. 471-477.